Journal of Energy Storage 105 (2025) 114715

Contents lists available at ScienceDirect

Journal of Energy Storage

journal homepage: www.elsevier.com/locate/est

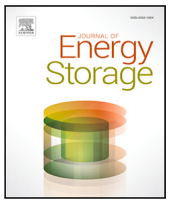

Research papers

Correlation analysis and feature extraction using impedance spectroscopy over aging of lithium ion batteries

Sebastian Pohlmann [a,*], Ali Mashayekh [b], Johannes Buberger [b], Julian Estaller [b], Andreas Wiedenmann [a], Manuel Kuder [c], Antje Neve [a], Thomas Weyh [b]

[a] University of the Bundeswehr Munich, Institute of Distributed Intelligent Systems, Werner-Heisenberg-Weg 39, Neubiberg, 85577, Bavaria, Germany
[b] University of the Bundeswehr Munich, Institute of Electrical Energy Systems, Werner-Heisenberg-Weg 39, Neubiberg, 85577, Bavaria, Germany
[c] BAVERTIS GmbH, Marienwerderstraße 6, Munich, 81929, Bavaria, Germany

ARTICLE INFO

Keywords:
Lithium-ion battery
State-of-health
Electrochemical impedance spectroscopy
Feature selection
Machine learning

ABSTRACT

To optimize the operation of batteries and to accelerate the transition to a renewable energy supply and sustainable transportation, it is crucial to determine the condition of Lithium-Ion Batteries at all time. A non-invasive tool for determining the State-of-Health of a battery cell is the electrochemical impedance spectroscopy, in which the impedance is calculated as a function of the excitation frequency. This paper presents a detailed correlation analysis between impedance and State-of-Health and, therefore, the dependency between capacity and impedance over the life cycle of a battery. After extensive testing series with 48 cells resulting in 25,344 impedance spectra, the highest correlations between the impedance and the State-of-Health could be obtained at a State-of-Charge of 10%. Further, features are extracted from the impedance based on their correlation to estimate the State-of-Health. To validate the results of the correlation analysis, a support vector regression and a multi-layer perceptron are trained and tested resulting in a mean absolute error of 0.86% and 0.84%. The estimation results confirm the correlation analysis and further substantiate the need for an appropriate feature extraction method.

1. Introduction

As the transportation sector is responsible for a large share of greenhouse gas emissions, it is crucial for the automotive and mobility industry to move to renewable energy [1]. Lithium-ion batteries (LIBs) have taken a predominant role as electrochemical energy storage solutions in many applications, ranging from portable consumer electronics to integration in power grids and battery electric vehicles (BEVs) [2]. Due to their high energy densities and their long lifespans, they are well suited for empowering BEVs [3]. Nevertheless, regardless of the application, LIBs degrade over time, which results in a loss of capacity and increase of internal resistance. To describe the aging condition, the battery State-of-Health (SoH) is used. The SoH is influenced by various intertwined factors as well as the high variety of operating and ambient conditions [4]. As LIBs are complex electrochemical systems, it is a key challenge to accurately predict the SoH. In the context of various degradation and failure mechanisms, this is a crucial task for a safe and reliable battery management system (BMS) [5]. Two main approaches can be distinguished for estimating the SoH: model-based and data-driven [6–8]. Data-driven approaches are gaining more and more interest as there is no need for the complex calculations to approximate the electrochemical processes in a battery cell [9]. Further, model parameters do not change over time and the efforts for using a single model for different cell chemistries can be reduced [10]. However, these data-driven models are highly depending on their data basis, which has to represent the battery behavior in reality. In combination with almost infinite possible loading and ambient conditions, this impedes the applicability of machine learning (ML) models [11]. A tool to analyze the internal electrochemical processes in a battery cell is the electrochemical impedance spectroscopy (EIS). This non-destructive testing method can improve the analysis of the condition of a battery, such as the State-of-Charge (SoC) or the SoH [12,13]. Further, it is possible to analyze lithium plating inside the cell, which is a main factor for the degradation of a LIB [14]. In galvanostatic mode, the impedance, which is analogous to the inhibition of current flow through a battery, is measured by observing the voltage response after a sinusoidal current excitation is applied to the cell [15]. The reverse is called potentiostatic mode. The result of the measurement is the complex valued impedance as a function of the frequency. Impedance data are indicators for internal electrochemical processes and can be used to determine the condition of the battery cell.

* Corresponding author.
E-mail address: sebastian.pohlmann@unibw.de (S. Pohlmann).

https://doi.org/10.1016/j.est.2024.114715
Received 2 September 2024; Received in revised form 13 November 2024; Accepted 17 November 2024
Available online 28 November 2024

In recent studies, a main focus lies on the usage of EIS data to estimate the SoH. As a battery cell ages, the impedance is increasing and the capacity is decreasing. The relationship between these two mechanisms can be used to estimate the SoH, which results in mainly data-driven approaches to predict the SoH or the remaining useful lifetime (RUL) [16,17]. Over the life cycle, the EIS measurements are conducted at the same condition, meaning the same SoC and the same temperature. This ensures the comparability of the impedance data, but it is not analyzed which is the most suitable condition to conduct an EIS measurement.

Zhang et al. used machine learning to identify degradation patterns based on impedance spectroscopy data [18]. They tested twelve battery cells and the dataset results in over 20,000 EIS spectra over three different constant temperatures and a varying SoC. The EIS measurements were each conducted following a 15 min rest after fully charging, right before discharging, after 10 min of discharging, after fully discharging, and after another 15 min period of resting time, respectively. The authors concluded that the measurements after resting are most suitable for estimating the SoH. While testing with four different cells, the coefficient of determination varied from 0.68 to 0.96 [18].

Obregon et al. used the same dataset and extracted features with a convolutional autoencoder from the EIS data; they then estimated the SoH with a deep neural network [19]. The dependence of EIS data on the SoC was beyond the scope of this publication and warrants future analysis. The lowest errors obtained were around 1.1% [19].

Jiang et al. analyzed four different cells during different aging conditions and measured 146 impedance spectra [20]. Three frequencies were selected based on the Pearson correlation, which is highest at the frequencies of 1 Hz, 5 Hz, and 10 Hz. The maximum estimation error over the life cycle could be obtained with 5.5%. Nevertheless, the authors concluded that the impact of SoC and temperature on the EIS characteristics has to be analyzed in order to improve the SoH estimation [20].

Chan et al. analyzed nine 18650 battery cells to estimate the SoH [21]. EIS data were used to conduct non-linear frequency response measurements. Based on the amplitude of the response, which has a higher increase at a high SoC, the authors concluded that high SoCs and low frequencies are most suitable for estimating the SoH. The investigated SoCs were 100, 80, 65, 50, 35, and 20%. It was noted that a detailed inspection of a suitable SoC should be conducted in the future. By calculating the Pearson correlation and the Spearman rank, specific features were selected to estimate the SoH, resulting in estimation errors around 0.75 to 1.5% [21].

Most of the approaches in the literature are using the data of EIS measurements at a specific condition over the life cycle. The data-driven models are especially dependent on the data that is used. While EIS measurements are highly influenced by parameters like the battery SoC or the temperature, there is no research about how the testing condition of EIS measurements and, therefore, the data basis can affect the accuracy of data-driven models. Zhang et al. are tackling the topic, but the time controlled and not condition controlled EIS measurements impede a detailed analysis [18]. The aim of this paper is to identify the most suitable condition for an EIS measurement with the focus of using the impedance data to estimate the SoH.

The contribution of this paper includes the in-depth correlation analysis between impedance data and the capacity-based SoH over battery aging for a total of 48 battery cells. In the context of data-driven estimation models for the condition monitoring of LIBs, the feature selection is a crucial part. The preparation of experiments and conditions to produce the data is of vital importance. This paper aims to identify the most suitable condition of a battery to estimate the capacity based on the impedance by means of data-driven models. Therefore, the batteries are analyzed under 16 different loading conditions and the correlations between the SoH and EIS data are calculated. During that, the influence of a varying SoC and different constant temperatures is analyzed. To the best of the authors' knowledge, this is the most detailed dataset of impedance data on the aging of battery cells resulting in 25,344 impedance spectra. There are approaches in the literature to estimate the SoH based on EIS data, but a detailed analysis of the impact on the battery condition is missing. Further, a detailed analysis of the SoC dependence on the EIS data and the impact on SoH estimation models is suggested. The dependency on the condition and the parameters of a battery impedes the estimation results. Because of the high efforts to obtain EIS data, the measurements in the literature are mainly conducted at the same condition over the aging of a battery without considering the optimal condition to determine the EIS. The comparability of the EIS measurements is ensured, but the possibility to improve the estimation of the battery condition based on EIS data is neglected. In this work, the correlation is calculated based on the Pearson correlation for linear relationships and the distance correlation for non-linear relationships between the real and the imaginary part as well as the SoH, respectively. The EIS measurements under different battery conditions are compared to identify the most suitable state to estimate the SoH. This includes a varying SoC in 10% intervals from 100% to 0%. After selecting the SoC with the highest correlations between the EIS data and the SoH, the individual frequencies consisting of the real and the imaginary part of the impedance are ranked based on the highest correlations. To verify the results, different machine learning models are trained, validated, and tested with the correlation-based feature extraction method. By adding single features to the model, the impact of the model dimension on the accuracy is determined. The detailed analysis is conducted using a support vector regression (SVR) and then further validated using a feedforward neural network (FNN). The detailed analysis of EIS data over battery aging can lead to improved battery diagnostics and can further reduce the measurement efforts to estimate an EIS via identifying the most suitable frequencies.

2. Materials and methods

In this section, the methodology from the experiments over the feature extraction to the ML models is described. First, the experiments, the test plan, and the hardware are presented. The section's main part is the feature extraction method based on the correlation between the impedance and the SoH. The indicators used are the Pearson correlation and the distance correlation. Finally, the ML models with support vector regression (SVR) and multi-layer perceptron (MLP) are explained.

2.1. Data origin

To obtain the data, the battery cell Molicel INR21700-P42A with a capacity of 4.2 Ah is tested in the battery test system OctoStat5000 from Ivium Technologies. This is a high current battery cell with a maximum discharge current of 45 A and a maximum operating temperature of 60 °C. The cathode consists of a lithium nickel manganese cobalt oxide (NMC). The battery test system combines the functionality necessary for the battery ageing experiments and the requirements for the check-up cycles with the EIS measurements. Therefore, the battery cells are fixed in battery holders and not moved during the whole experiments. The battery tests are conducted in two Binder climate chambers at a constant temperature of 23 °C and 50 °C, respectively. Under 16 different conditions, three cells were tested per condition to ensure accurate measurements and reproducibility of the results, resulting in a total of 48 battery cells tested. In addition to DC loading, a sinusoidal loading pattern to simulate pulse loading is used to charge and discharge the battery cells. The frequency is varied between 10 Hz, 100 Hz, 1 kHz, and 10 kHz. The current for the DC loading is 2 A, while for the AC loading, a DC current with an amplitude of 2 A is overlayed with the 2 A AC current. During cycling, the depth of discharge (DoD) is varied between a SoC of 20% to 50% and 50% to 90%. The testing conditions are summarized in Fig. 1.

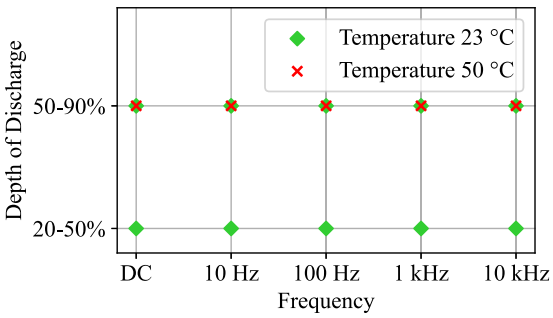

Fig. 1. Loading conditions during aging tests of the battery cells. Three cells each are tested under the same loading conditions.

In addition to the 45 cells used under the 15 loading conditions shown in Fig. 1, the remaining three cells are loaded with a DoD of 20%–70% at a temperature of 50 °C and a frequency of DC, 1 kHz, and 10 kHz.

After every 50 cycles of the aging tests, a check-up cycle is performed. The cells are tested for 750 aging cycles, resulting in 16 check-up cycles. During the check-ups, EIS measurements are conducted after discharging the battery in 10% intervals from a SoC of 100% to 0%. Again, these EIS measurements are repeated three times to identify measurement errors. In addition, a capacity test is conducted during the check-up cycles, in which the SoH is calculated using Eq. (1). The SoH is the ratio between the actual available capacity Q_{now} and the initial capacity at the begin of life Q_{BoL}.

$$SoH = \frac{Q_{now}}{Q_{BoL}} \tag{1}$$

In total, the dataset consists of 48 cells with 16 check-ups and three times eleven EIS measurements during a check-up, resulting in 25,344 EIS curves representing the condition of the battery cells. The impedance spectra over aging for an exemplary cell is shown in Fig. 2. The shown EIS measurements were conducted at a SoC of 10% for Fig. 2(a) and 100% for Fig. 2(b), both at a constant temperature of 23 °C. The corresponding SoH is color-coded. During the EIS measurements, 48 frequencies between 5 kHz and 0.1 Hz were analyzed. Out of three repetitive measurements for each cell and condition, the results of the first one in each case are exemplary shown in Fig. 2. The plot shows the EIS measurements of the same cell during the check-up cycles, just at a different SoC. Although, the change of the impedance over aging is clearly visible at a SoC of 10% and 100%, as expected, the impact of the aging on the impedance curve vary between the SoCs. This indicates that the suitability of EIS data for estimating the capacity vary between the different conditions.

2.2. Feature extraction

The feature extraction of the raw EIS data is conducted by the means of two different correlation values. The Pearson correlation, which is an indicator for the linear relationship between two variables, and the distance correlation, which calculates the linear and non-linear association between two variables. For the Pearson correlation, the value range is between −1 and +1, where +1 indicates a perfect positive and −1 a negative correlation between two variables. The value range of the distance correlation is from 0 to 1. A value close to zero indicates a weak correlation between two variables, which applies to both coefficients. The corresponding equation for the Pearson correlation r is shown in Eq. (2) and for the distance correlation $dCor$ in Eq. (3). With two different variables $(x_1, \dots, x_n)$ and $(y_1, \dots, y_n)$, the Pearson correlation r is calculated with the corresponding mean values $\overline{x}$ and $\overline{y}$. The distance correlation $dCor$ in (3) is defined as the ratio between the distance covariance $dCov$ in (4) and the distance variance

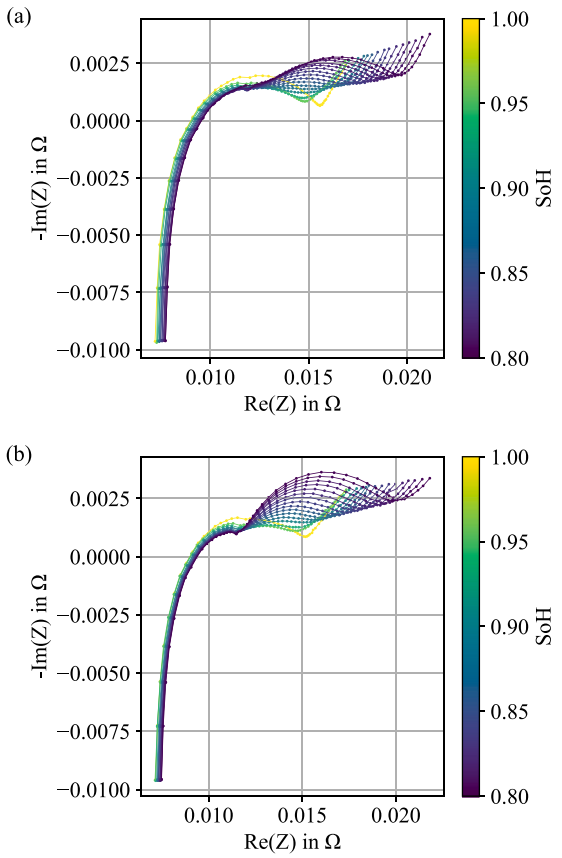

Fig. 2. Nyquist plot of one out of 48 tested battery cells. The shown impedance spectra are at a SoC of 10% (a) and a SoC of 100% (b). The corresponding SoH is color-coded.

$dVar$ in (10) [22,23]. A and B are distance matrices containing the pairwise distances between the variables x and y shown in (5) and (6). The distance matrices are centered in (7) and (8) with the mean of ith row $\bar{a}_{i\cdot}$, the mean of the jth column $\bar{a}_{\cdot j}$, and the grand mean of distance matrix $\bar{a}_{\cdot\cdot}$. The corresponding equations for calculating the terms are exemplary shown for A in (9). The distance variance $dVar$ is the special case, where the variables of the distance covariance $dCov$ are identical.

$$r = \frac{\sum_{i=1}^{n}(x_i - \overline{x})(y_i - \overline{y})}{\sqrt{\sum_{i=1}^{n}(x_i - \overline{x})^2}\sqrt{\sum_{i=1}^{n}(y_i - \overline{y})^2}} \tag{2}$$

$$\mathrm{dCor}(x, y) = \frac{\mathrm{dCov}(x, y)}{\sqrt{\mathrm{dVar}(x) \cdot \mathrm{dVar}(y)}} \tag{3}$$

$$\mathrm{dCov}^2(x, y) = \frac{1}{n^2}\sum_{i,j} A_{ij} B_{ij} \tag{4}$$

$$a_{ij} = \|x_i - x_j\| \tag{5}$$

$$b_{ij} = \|y_i - y_j\| \tag{6}$$

$$A_{ij} = a_{ij} - \bar{a}_{i\cdot} - \bar{a}_{\cdot j} + \bar{a}_{\cdot\cdot} \tag{7}$$

$$B_{ij} = b_{ij} - \bar{b}_{i\cdot} - \bar{b}_{\cdot j} + \bar{b}_{\cdot\cdot} \tag{8}$$

$$\bar{a}_{i\cdot} = \frac{1}{n}\sum_{j=1}^{n} a_{ij}, \quad \bar{a}_{\cdot j} = \frac{1}{n}\sum_{i=1}^{n} a_{ij}, \quad \bar{a}_{\cdot\cdot} = \frac{1}{n^2}\sum_{i,j=1}^{n} a_{ij} \tag{9}$$

$$\mathrm{dVar}(X) = \mathrm{dCov}(X, X) \tag{10}$$

For the Pearson correlation, three areas can be separated. The low correlation area between 0 and |0.3|, medium correlation between |0.3| and |0.7|, and high correlation between |0.7| and |1|.

Before the training of the estimation models is conducted, the dataset is divided into a training, a validation, and a test set. The validation set is used to select a suitable kernel function for the SVR and to optimize the hyperparameter of the artificial neural network (ANN). The dataset is first divided into a training and test set with a ratio of 80:20 and the training set is then subdivided into a final training and validation set with a ratio of 90:10. Based on the training data, all three datasets are normalized into an interval between zero and one before they are used in the estimation models.

2.3. Machine learning model

Two different ML models are trained based on the correlation feature extraction method. The first one is an SVR and the second one is an MLP. The SVR is chosen because of the characteristics of the dataset. The dataset is comparably small in the ML domain and has a small amount of features. The SVR, as a more conventional ML model, is efficient and stable for this kind of data. Further, it has less hyperparameters to tune and, due to the nature of the SVR, it can partially prevent overfitting. However, there is a trend in the approaches in the literature to use artificial neural networks (ANNs) [24–26]. Similar to the SVR, a simple ANN with the MLP is used due to the dataset characteristics. Further, this reduces computational efforts, as the model has to be retrained several times to validate the feature extraction method. The results of the ML models are compared using the mean absolute error (MAE) shown in (11) and the coefficient of determination R^2 in (12) with the real target values y_i, the estimated target values y_i^*, and the mean of the real target values $\bar{y}^2$.

$$MAE(y_i, y_i^*) = \frac{1}{n}\sum_{i=1}^{n}|y_i - y_i^*| \tag{11}$$

$$R^2(y_i, y_i^*) = 1 - \frac{\sum_{i=1}^{n}(y_i - y_i^*)}{\sum_{i=1}^{n}(y_i - \bar{y})^2} \tag{12}$$

2.3.1. Support vector regression

A SVR is closely related to a support vector machine (SVM) for classification. An n-dimensional hyperplane is to be determined for an optimized separation of data points. While maximizing the distance between the nearest data points and the hyperplane, the model is trained. In an SVR, in contrast, the hyperplane is used to approximate the data. Instead of maximizing the distance to the hyperplane, it is minimized. With given training data (x_i, y_i), the aim is to find a function $f(x)$ that predicts the target values within an error margin ϵ. To handle outliers of the error margin, two terms ζ_i and ζ_i^* are introduced to penalize the objective, depending on the prediction and the error margin. The objective function with a regularization parameter C for minimizing the norm of the weight vector w is shown in Eq. (13) [27].

$$min_{w,\zeta_i,\zeta_i^*}(\frac{1}{2}\|w\|^2 + C\sum_{i=1}^{n}(\zeta_i + \zeta_i^*)) \tag{13}$$

To solve the dual formulation of the problem, the objective function can be transformed using Lagrange multipliers α_i and α_i^* as well as a kernel function K. This results in Eq. (14) with the bias vector b [28].

$$f(x) = \sum_{i=1}^{n}(\alpha_i - \alpha_i^*)K(x_i, x_j) + b \tag{14}$$

By means of the kernel function, the feature space can be transformed into a higher dimension, which enables linear estimations in a higher dimensional feature space to determine non-linear relations. This is called the Kernel-trick. The radial basis function (RBF) is mainly used in approaches to estimate the SoH [29,30]. The RBF with the width γ is shown in Eq. (15) [31].

$$k_\gamma\left(x, x^*\right) = e^{-\frac{\|x-x^*\|_2^2}{\gamma^2}}, \quad x, x^* \in \mathbb{R} \tag{15}$$

Table 1
Hyperparameters of the SVR used to estimate the SoH based on EIS data.

Hyperparameter	Value
Kernel	RBF
Degree kernel function	5
ϵ-tube	0.01
Penalty parameter	2.0

Table 2
Hyperparameters of the MLP used to estimate the SoH based on EIS data.

Hyperparameter	Value
Hidden layer	2
Neurons hidden layer 1	20
Neurons hidden layer 2	20
Activation function	ReLU
Optimizer	Adam
Epochs	100

The used parameters of the SVR are summarized in Table 1. The ϵ-parameter describes the distance tube from the predicted to the actual value, where no penalty is awarded during the training of the model. The penalty parameter describes the impact of the penalty outside the ϵ-tube.

2.3.2. Multi-layer perceptron

In addition to the SVR, an ANN is used to estimate the SoH based on EIS data. For that, a simple form of ANNs with an MLP is used. This is a FNN in which the flow of information from the input to the output layer takes place in one direction. As the main focus of this work lies on the feature selection, the efforts for the hyperparameter optimization is kept at a medium level. Therefore, a grid search is performed to obtain the number of neurons, the activation function, and the optimizer algorithm. There are several approaches in the literature for estimating the SoH of LIBs, which suggest the usage of an MLP with only one or two hidden layers regarding computational cost and accuracy of the model [32–34]. The structure of the used MLP consists of two hidden layers with 20 neurons in each layer. As activation function, the rectified linear unit (ReLU) function and, as optimizer, the Adam algorithm is used [35]. By means of the backpropagation algorithm, the weights are adjusted and the MLP is trained. The maximum amount of iterations is set to 100. The hyperparameters are determined by using the training and the validation data. They are summarized in Table 2.

3. Results

The results are divided into two main sections. The first one is the correlation analysis of EIS data with the SoH. The second one is the SoH estimation based on the extracted features with the SVR and the ANN.

3.1. Correlation analysis

The Pearson correlation and the distance correlation between each real and imaginary part, individually, and the SoH is calculated. While analyzing the impedance with real and imaginary part at 48 frequencies, this results in a correlation vector with the length 96 for one SoC. This is done for each EIS measurement and then averaged for each SoC resulting in a correlation matrix with the dimension 11 times 96. By that, the SoC with the highest correlation to the SoH is obtained. A histogram of all correlation values over |0.7| is shown for the Pearson correlation in Fig. 3.

First of all, it is noticeable that a high amount of linear correlations can be found in the EIS data. The highest amounts are at the start of discharging with a SoC of 100% and at a SoC of 10%. In contrast,

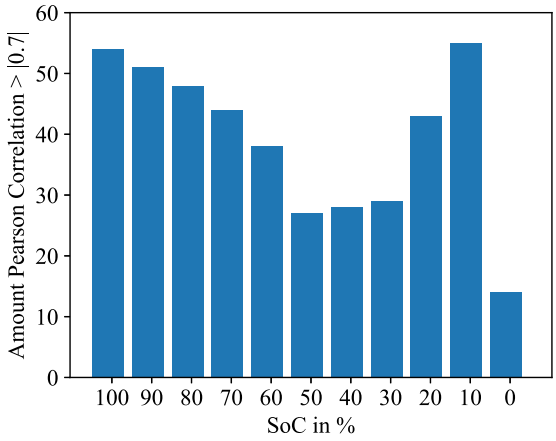

Fig. 3. Histogram of Pearson correlation value over |0.7| for each SoC. Each value is the correlation between the real or imaginary part of the different frequencies and the SoH. In total, 96 correlation values per SoC are calculated. The correlations are the mean values over all different loading conditions calculated at the same SoC.

a SoC of 0% shows the least correlations. Between a SoC of 100% and 10%, the amount of high correlations first decreases with the lowest values at 50% and then increases again until a SoC of 10%. Next to the Pearson correlation with higher variations between the different SoCs, the distance correlation is similar for every SoC. The detailed correlation matrix for both indicators is shown in Fig. 4. In the heat map, on the x-axis, the real and imaginary parts of the impedance are alternately shown for each frequency. On the y-axis, the eleven analyzed SoCs are presented. The correlation of each real and imaginary part of the impedance to the SoH is indicated by the color. In Fig. 4(a), the Pearson correlation and in Fig. 4(b), the distance correlation is presented, respectively.

The Pearson correlation values vary from −1 with a negative correlation to +1 for a positive correlation. Based on the linear correlation, it is notable that the real and the imaginary parts of the impedance at high frequencies are highly negatively correlated to the SoH. There are slight differences, but the highest values can be observed at a SoC of 100%. After that, the correlation is drifting to a positive value, but it is alternating between the real and imaginary part. The highest correlations in the mid and low frequency areas can be seen at a SoC of 10%. Next to that, an area of low correlations can be observed for the SoC range from 90% to 20%. Even though SoC 100% and 10% show a similar behavior, SoC of 10% has slightly higher correlations. Further, at a SoC of 0%, the correlations are lower compared to the other states. Looking at the distance correlation, the constant behavior over all SoCs is particularly notable. The distance correlation has the lowest values in the high frequency area. After that, the highest correlations can be observed in the mid frequency area. In the low frequency area, the correlations are slightly decreasing again, but they stay nearly constant. For both correlation indicators, the alternating behavior for the real and imaginary parts can be seen. A detailed view of the distance correlation is depicted in Fig. 5.

Several points are striking in the correlation curve. First of all, the imaginary part has a lower correlation to the SoH in the high frequency area. In the mid frequency area, three minima, two of the real part and one of the imaginary part, can be observed. The minima of the real part are roughly at the first quarter of the semi-circles, while the minima including the imaginary part of the impedance can be found at the start of the second semi-circle. Next to the minima of the imaginary part, the highest correlations can be observed. In the low frequency area, the correlations of the impedance's real and imaginary part to the SoH are nearly the same. In sum, the distance correlations is greater than 0.6 across the whole spectrum. The highest values were calculated for the imaginary part in the mid frequency area. The correlation analysis is used to extract features for the ML models. Based on the shown results, the real and imaginary part of the impedance are ranked according to their correlation starting with the highest values. The models are then trained and tested with the first feature. Step by step, the features are added to validate the usability of the correlation analysis.

3.2. State of health estimation

After performing the correlation analysis, the features are ranked depending on the absolute value of the correlation. Then, both models are trained with the feature with the highest correlation. Step by step, a feature is added based on the distance correlation. The maximum amount of features is set to 50, as the errors are slightly increasing after reaching the minimum. By adding the features one by one, the correlation analysis is validated and the need for a feature selection is proven. The whole process is repeated for each SoC to identify the most suitable SoC for estimating the SoH and to compare the results of the correlation analysis to an estimation model. The results of the SVR are demonstrated in Fig. 6. The shown errors result from the testing set, which the model has not seen during the training phase.

Similar to the correlation results, the lowest estimation errors can be obtained for a SoC of 100% and 10%. While the model based on the EIS data at a SoC of 100% reaches errors below 1% with 30 features, the model with the EIS data at SoC of 10% only needs eleven features for errors below 1%. In the following, the lowest error can be obtained with a value at 0.86% with 30 features. Nevertheless, the error results at a SoC of 0% exceed all other states for every amount of features. Further, it can be seen for all states that the error is first decreasing since a minimum is reached; after that, the error is increasing again. This is more pronounced for some states like SoC of 80%, but visible for all curves. The fluctuations are higher in the mid SoC area. The results with the data of SoC 10% show the smoothest curve and the lowest error.

The results of the correlation analysis and the SVR are further compared to an MLP. The results of the MLP are shown in Fig. 7. Similar to the presentation of the SVR results, the used EIS data and the corresponding SoC are indicated by color. The MAE is shown over the amount of features used to train the model.

In comparison to the SVR, higher fluctuations are visible. The impact on the model by adding features is higher compared to the SVR. Further, the errors are slightly higher, especially in the mid SoC area, where a convergence to a minimum is hard to detect. On the contrary, the errors of these curves are more or less constant neglecting the fluctuations, which are increasing with an increasing amount of used features for the model. Similar to the results of the SVR, the best results are obtained with the EIS data at a SoC of 10%. The lowest error is at 19 features with a MAE of 0.84%. However, this is the only obtained test error below 1%. Nevertheless, the results of the MLP confirm the results of the SVR and the feature extraction method based on the correlation. As the SVR shows more robust behavior, the final model with 30 features is used to estimate the SoH for single cells. The results only show the testing error. The model is trained with all cells at all conditions except for one. Then the model is tested at a single cell of the non-trained condition. This was repeated for all cells. The results of two exemplary cells with the R^2-score and the MAE are shown in Fig. 8.

There is variation between the test errors for each cell varying around the MAE of 0.86%. Next to that, the mean value of the R^2-score is 0.88. This shows the high impact of a suitable feature extraction method. Without a detailed model optimization, a high accuracy can be obtained by selecting the right features.

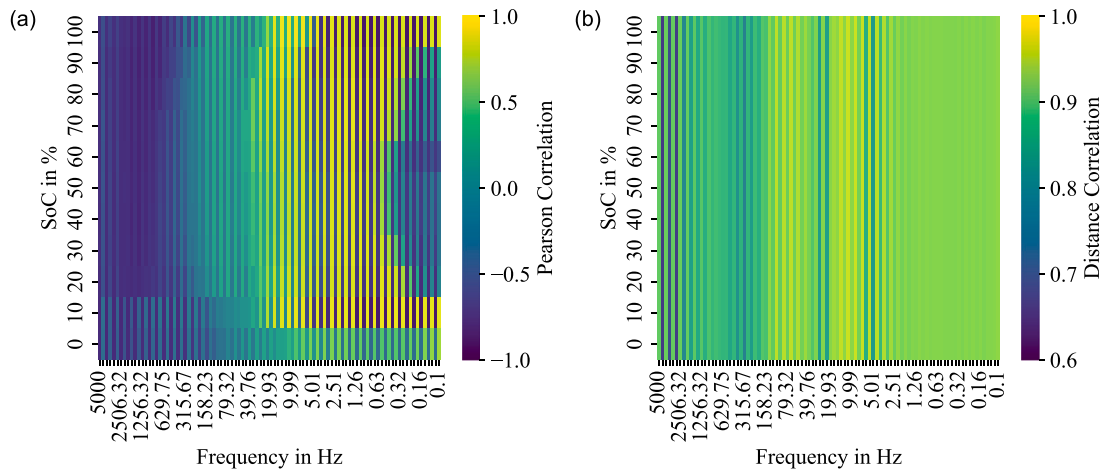

Fig. 4. Heat map of the Pearson Correlation (a) and the distance correlation (b). The correlation is calculated between the real and imaginary part of the impedance and the SoH. Each shown value is the averaged value of each condition for the same SoC. The real and imaginary parts are alternating for the frequencies. For reasons of clarity, only every sixth frequency value is shown on the x-axis.

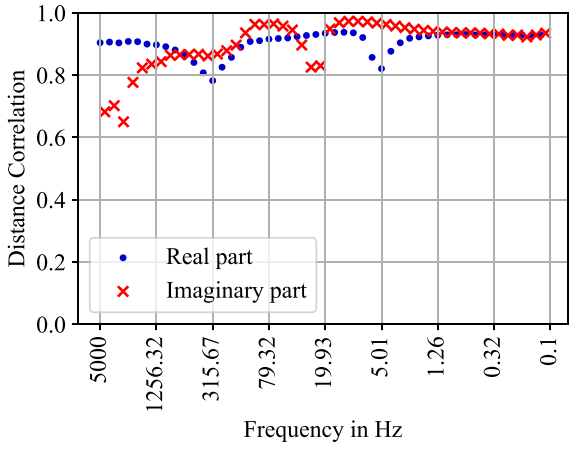

Fig. 5. Distance correlation of the impedance's real and imaginary parts for all frequencies at a SoC of 10%.

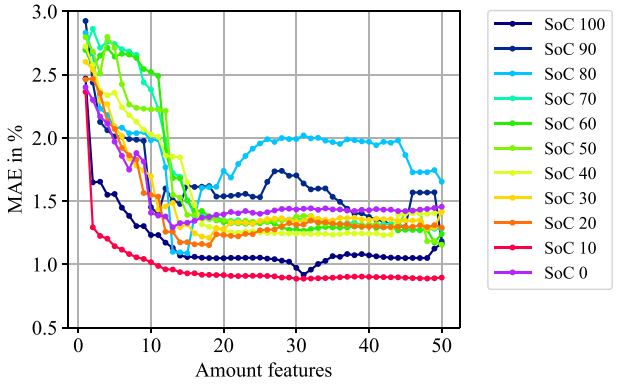

Fig. 6. Test results of the SVR using the EIS data at different SoCs. The input features are ranked based on their correlation coefficient to the SoH. Successively, the features are added and the model is retrained and tested.

4. Discussion

Two different correlation coefficients are used to extract features from EIS data to estimate the SoH of LIBs. The Pearson correlation is used to determine the optimal condition of the battery to estimate

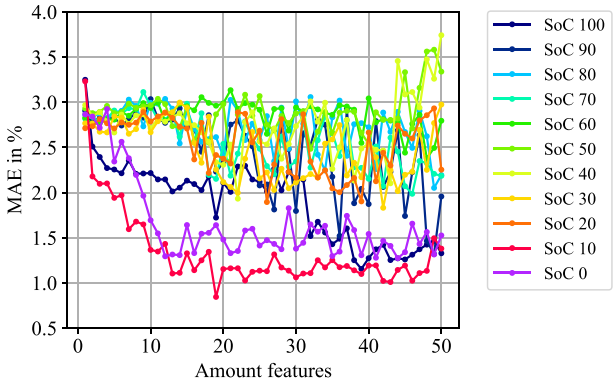

Fig. 7. Test results of the MLP using the EIS data at different SoCs. The input features are ranked based on their correlation coefficient to the SoH. Successively, the features are added and the model is retrained and tested.

Table 3
Test protocol for the EIS measurements of [18].

State	Description
5	After charging and 15 min rest
6	Start discharging
7	After 10 min discharging
8	After discharging and before resting
9	After 15 min rest

the SoH. Because most studies do not analyze the influence of the battery SoC on the results of SoH estimation models, it is unclear which state is most suitable for estimating the SoH. The need for extensive hardware for EIS measurements and the differences in needs between EIS measurements and comparable simple aging tests impedes the task.

4.1. Comparison public dataset

While most studies are performing EIS measurements at the same condition to compare the development of the EIS data, Zhang et al. [18] compared the EIS data at different states. However, they performed the EIS measurements at a predefined time, which complicates the comparability regarding the SoC. Nevertheless, the results of the Pearson correlation and the distance correlation are shown in Fig. 9. The battery states at which the EIS measurements were conducted are summarized in Table 3 [18].

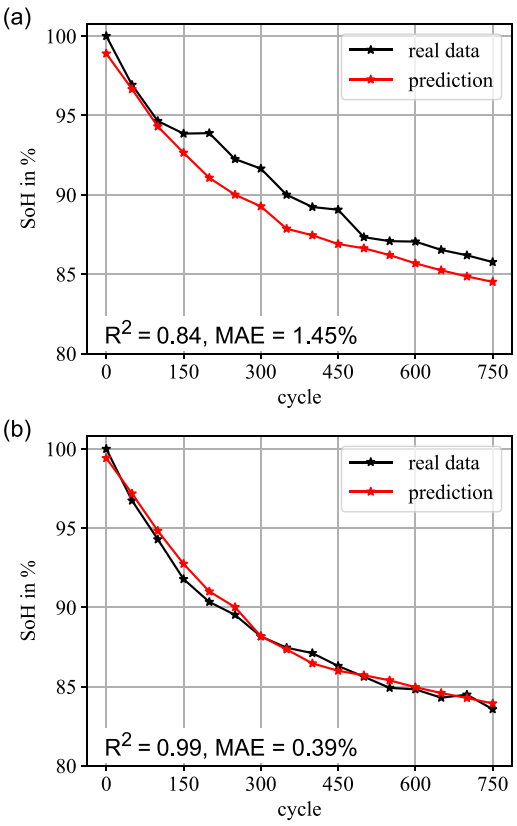

Fig. 8. Test results of two exemplary cells for the SoH estimation. The real target values are marked in black and the predicted values are shown in red. The corresponding coefficient of determination and the MAE are displayed in the lower left of each plot. (For interpretation of the references to color in this figure legend, the reader is referred to the web version of this article.)

Although it is not possible to directly compare the results, it is notable that there are higher correlations in the states six, seven, and eight. These are the states directly before, during, and after discharging. This indicates that the resting periods are not necessary. Further, looking at the distance correlations, which were constant over the SoC in our findings, similar behavior can be obtained. There are differences, but smaller ones compared to states five and nine. Zhang et al. state that the low-frequency area is most relevant for an SoH estimation [18]. This is similar to the correlation analysis in this paper. Even though the batteries are discharged with 2C and are, therefore, varying to this testing plan, the correlation areas are similar. We expect the impact of the charging or discharging rate to not be significant if all intervals are charged or discharged with the same C-rate. Next to that, high correlations could be observed in the mid-frequency area, which enhances the possibilities for the feature extraction and could further reduce the necessary time of an EIS measurement. Further, at state seven, the highest distance correlations can be seen in the mid frequency area, similar to our findings. However, it must be taken into account that the frequency range is not the same. In the low frequency area, the distance correlation is comparably lower. Considering the other frequencies and the changing battery condition for the EIS measurement during discharging, a similar behavior can be obtained.

4.2. Correlation based feature extraction

Conventional EIS measurements are very time consuming. Using only medium frequencies for estimating the SoH of a LIB could benefit the measurement efforts. By considering the estimation results of SVR and ANN, it can be concluded that the medium frequencies are sufficient to estimate the SoH based on EIS data. The SVR falls below an MAE of 1% after 11 features and the ANN with 19 features. Comparing the amount of features with the correlation analysis, it shows that nearly all features for the estimation are located in the mid frequency area. Further, the feature selection and the increasing error after the minimum while adding features substantiate the need for a feature extraction method. A possible explanation for the higher correlation in the mid frequency area are the electrochemical processes in the cell, which are more distinct during discharging. These processes within a cell, for example charge transfer and solid electrolyte interphase formation, are represented in the mid frequency area. This is an indicator for the aging of a cell. It is striking that the highest correlations are obtained for a SoC of 10% in the mid frequency area.

Commonly, the EIS measurements are performed at a SoC of 100% to reach a stable condition of the battery [36,37]. To compare the development of EIS data, it is important to analyze the cell at the same condition over the aging cycle, but the most suitable point to estimate the SoH is not determined. The efforts for time and hardware complicate detailed studies. The requirements for EIS measurement hardware are much higher than for battery aging test systems. In most studies, this hardware is separated, which further increases the efforts for testing [38,39]. The manual tests and the physical relocation of cells between test systems can affect the measurements. The experiment setup in this paper enables both measurements on the same hardware and the possibility to determine the most suitable condition of the batteries to correlate the impedance to the SoH.

Comparing the EIS data at a SoC of 100% to 10%, the correlations are lower and the estimation results are slightly worse. Nevertheless, for the SVR, the second best results, and for the ANN, the third best results were determined. Performing the EIS measurements at a SoC of 100% simplifies the experiments, as there is no need to charge or discharge the cells to a certain SoC. However, looking at the correlation values and the estimation results, the efforts for doing that can be worth it. The amount of features can be drastically reduced and the accuracy can also be increased. The low correlations in the medium SoC range are mainly influenced by the imaginary part of the impedance. Looking at the Nyquist plots in Fig. 2, the imaginary part at the lowest frequencies increases during aging. For the measurements at a medium SoC, the imaginary part at the lower frequencies is nearly constant and there is no trend visible over the degradation of the batteries. This is probably caused by the unstable chemical condition of the battery during discharging. Even though the increased imaginary part at low frequencies during degradation is apparent at the measurement for a high and low SoC, the measurements at a SoC of 0% has also low correlations. This is caused by another phenomenon. While for every other SoC, the degradation with an increasing impedance is clearly visible, the impedance curves at a SoC of 0% are mainly overlapping for roughly the first 300 cycles. Only afterwards, the degradation is clearly visible in the Nyquist plot. Therefore, the correlation results are also low in comparison to the measurements at other SoCs.

Looking at the feature extraction based on the distance correlation in detail, it is notable which frequencies in the spectra have the minima in the correlation curve. While analyzing the EIS data over aging, as shown in Fig. 2, in the high frequency area, the deviations in the real part of the impedance are visible. After the intersection point with the x-axis, there is a shift and the main deviations can be obtained for the imaginary part. This shift can also be seen in the correlation data, in which the first local correlation minimum is reached for the real part while the correlation for the imaginary part is increasing. The imaginary part's correlation minimum is reached in the frequency region, where the curves drift apart regarding the SoH. This area contains a switch in the order from highest to lowest imaginary part of the impedance regarding the SoH. The second local minima can be located in the end of the mid frequency area. As the semi-circles are more pronounced based on the SoH, there are higher deviations in the real part, which could impede the correlation results.

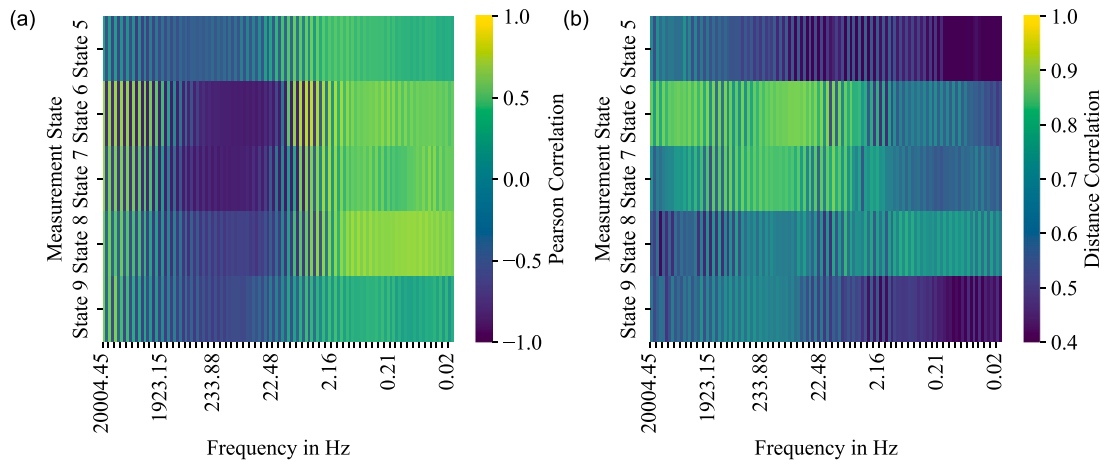

Fig. 9. Heat map of the Pearson Correlation (a) and distance correlation (b) calculated with the data from [18]. The correlation is calculated between the real and imaginary part of the impedance and the SoH. Each shown value is the mean for the same SoC. The real and imaginary parts are alternating for the frequencies. For reasons of clarity, only every sixth frequency value is shown on the x-axis.

4.3. State-of-health estimation

The SoH estimation based on EIS data is performed using an SVR and an MLP. The efforts to optimize the models is kept at a medium level as the main focus lies on the correlation analysis and the feature extraction. Both models are trained and tested to validate the feature extraction method. Nevertheless, several points in the estimation results are striking. The results of the MLP are noisier than the SVR. The SVR is more robust against changing input data. Further, the SVR falls below a MAE of 1% with eleven features, while the MLP needs 19 features. Even though the lowest error was obtained with the MLP, the SVR shows an overall better performance. The deviations while adding features impedes the reliability of the MLP. The MLP has more hyperparameters to tune, and there are higher deviations while retraining the model. Without further regularization methods, the fluctuations increase with more input features. This substantiates the need for a suitable feature extraction method. However, the relatively small MLP is sufficient to estimate the SoH based on the EIS data. In comparison to that, the SVR shows similar but more stable results. Initially, the errors decrease when adding features, and after the minimum is reached, the error increases. This indicates that conventional ML algorithms are sufficient to capture the relationship between impedance and capacity. The results of both estimation models validate the results of the correlation analysis. The EIS data with an SoC of 10% leads to the highest accuracies. The EIS data of SoC 100%, which has the second highest correlations, has the second best accuracies for the SVR and the third highest accuracies for the MLP. However, a deviation for the SoC of 0% can be observed. While it has the lowest values for the Pearson correlation, the results of the estimation models trained with the EIS data at a SoC of 0% exhibit comparably good results. Even though the correlation values are in a close range, the results were not expected. The impact of the feature extraction method can clearly be seen. It is possible to halve the error by using suitable features. Nevertheless, nearly all models result in errors below 3.5%. Without optimizing the final model, the errors can be reduced from roughly 3% to under 1% by extracting suitable features. The impact of the SoC during the EIS measurements can be clearly seen in the estimation results.

Overall, EIS data is highly suitable to estimate the remaining capacity of a LIB. By choosing a feature extraction method, the accuracies of the models can be increased and the measurement efforts can be reduced. The highest correlations can be observed at a SoC of 10% and the second-highest at a SoC of 100%. Only by using the data at a suitable condition, the SoH estimation could be clearly improved. In an application, it could be beneficial to measure the impedance data at a SoH of 100%, as it is not necessary to discharge the batteries to a specific SoC. The slightly lower accuracy is a compromise to reduced measurement efforts. On the contrary, the EIS measurements at a medium SoC area are not suitable for estimating the SoH. Next to that, the individual frequencies were analyzed to further reduce the complexity of the model and increase the accuracy. Despite local minima, the highest correlation could be observed in the mid-frequency area. Especially the amount of low frequencies can be reduced through the feature extraction method, which would benefit the measurement time. The impedance in the mid frequency area exhibits similar and higher correlations to the SoH. Even though the models were not optimized in detail, errors below 1% could be reached. It is expected that further optimized models could reach even higher accuracies. Comparing the estimation results to models in the literature, it is striking that similar and slightly higher accuracies could be reached with simpler models. While the R^2 has the mean value of 0.88 over all cells and most of the cells are in the range between 0.82 and 0.94, single cells reach a value of 0.99. Zhang et al. obtain R^2-scores from 0.72 to 0.88 for the capacity estimation with a gaussian process regression and an automatic relevance determination kernel [18]. Even though the SVR is less complex, similar and higher accuracies could be obtained for the SoH estimation model. Especially in comparison to accuracies from models in the literature, the results emphasize the high impact of the feature extraction method and the optimization potential of data-driven models by selecting the most suitable features.

5. Conclusion

LIBs undergo unpreventable aging during their life cycle. Thereby, the capacity is decreasing and the impedance is increasing. There are various degradation mechanisms and the battery parameters are highly inter-correlated. Yet, it is crucial to determine the condition to optimize the operation of LIBs. A suitable tool to determine the impedance of a cell is the EIS. High measurement efforts impede the feasibility in practice and detailed research studies. After conducting comprehensive test series for battery aging and check-up cycles, resulting in 25,344 impedance spectra over the life cycle of 48 battery cells, the data is analyzed to determine the highest correlation between the impedance and the SoH. The Pearson correlation is used to find the most suitable SoC to conduct the EIS measurements for estimating the SoH. Based on the amount of high correlations and the correlation itself, a SoC of 10% was identified. After that, the distance correlation was used to extract features from the impedance spectra. Especially the mid frequency area exhibited high correlations, while keeping the measurement time low in comparison to the low frequency area. After ranking the real and imaginary part of the impedance based on their correlation to the SoH

and adding the features step by step to the models, a lowest test MAE of 0.86% for the SVR and 0.84% for the MLP could be obtained. The results show that even simpler models can reach higher accuracies in comparison to approaches from the literature by selecting the most suitable features. This substantiates the need for an advanced feature extraction method and further demonstrates the high impact of the data pre-processing step on estimation models.

In the future, it is planned to further optimize the models and to further increase the accuracies of the estimations while expanding the dataset. Regarding sustainability, it is important to optimize the operation of LIBs by finding the most suitable point to estimate their condition.

CRediT authorship contribution statement

Sebastian Pohlmann: Writing – original draft, Visualization, Validation, Software, Resources, Methodology, Investigation, Formal analysis, Data curation, Conceptualization. **Ali Mashayekh:** Writing – review & editing, Resources, Methodology, Investigation, Formal analysis, Data curation, Conceptualization. **Johannes Buberger:** Writing – review & editing, Validation, Methodology, Investigation, Formal analysis. **Julian Estaller:** Writing – review & editing, Validation, Methodology, Investigation, Formal analysis. **Andreas Wiedenmann:** Writing – review & editing, Validation, Methodology, Investigation. **Manuel Kuder:** Writing – review & editing, Supervision, Project administration, Funding acquisition. **Antje Neve:** Writing – review & editing, Visualization, Supervision, Project administration, Funding acquisition, Formal analysis. **Thomas Weyh:** Writing – review & editing, Supervision, Project administration, Funding acquisition.

Declaration of competing interest

The authors declare that they have no known competing financial interests or personal relationships that could have appeared to influence the work reported in this paper.

Acknowledgment

This research [project MORE] is funded by dtec.bw – Digitalization and Technology Research Center of the Bundeswehr, which we gratefully acknowledge. dtec.bw is funded by the European Union – NextGenerationEU.

Data availability

Data will be made available on request.

References

[1] J. Buberger, A. Kersten, M. Kuder, R. Eckerle, T. Weyh, T. Thiringer, Total CO2-equivalent life-cycle emissions from commercially available passenger cars, Renew. Sustain. Energy Rev. 159 (2022) 112158.

[2] W. Bernhart, Challenges and opportunities in lithium-ion battery supply, in: Future Lithium-Ion Batteries, The Royal Society of Chemistry, 2019, pp. 316–334, http://dx.doi.org/10.1039/9781788016124-00316.

[3] S. Stock, S. Pohlmann, F.J. Günter, L. Hille, J. Hagemeister, G. Reinhart, Early quality classification and prediction of battery cycle life in production using machine learning, J. Energy Storage 50 (2022) 104144, http://dx.doi.org/10.1016/j.est.2022.104144, URL https://www.sciencedirect.com/science/article/pii/S2352152X22001785.

[4] A. Basia, Z. Simeu-Abazi, E. Gascard, P. Zwolinski, Review on state of health estimation methodologies for lithium-ion batteries in the context of circular economy, CIRP J. Manuf. Sci. Technol. 32 (2021) 517–528, http://dx.doi.org/10.1016/j.cirpj.2021.02.004, URL https://www.sciencedirect.com/science/article/pii/S1755581721000249.

[5] G.-W. You, S. Park, D. Oh, Diagnosis of electric vehicle batteries using recurrent neural networks, IEEE Trans. Ind. Electron. 64 (6) (2017) 4885–4893, http://dx.doi.org/10.1109/TIE.2017.2674593.

[6] J. Li, S. Zhao, M.S. Miah, M. Niu, Remaining useful life prediction of lithium-ion batteries via an eis based deep learning approach, Energy Rep. 10 (2023) 3629–3638, http://dx.doi.org/10.1016/j.egyr.2023.10.030, URL https://www.sciencedirect.com/science/article/pii/S2352484723014592.

[7] C. Li, L. Yang, Q. Li, Q. Zhang, Z. Zhou, Y. Meng, X. Zhao, L. Wang, S. Zhang, Y. Li, F. Lv, SOH estimation method for lithium-ion batteries based on an improved equivalent circuit model via electrochemical impedance spectroscopy, J. Energy Storage 86 (2024) 111167, http://dx.doi.org/10.1016/j.est.2024.111167, URL https://www.sciencedirect.com/science/article/pii/S2352152X24007515.

[8] Z. Ren, C. Du, A review of machine learning state-of-charge and state-of-health estimation algorithms for lithium-ion batteries, Energy Rep. 9 (2023) 2993–3021, http://dx.doi.org/10.1016/j.egyr.2023.01.108, URL https://www.sciencedirect.com/science/article/pii/S235248472300118X.

[9] H. Tian, P. Qin, K. Li, Z. Zhao, A review of the state of health for lithium-ion batteries: Research status and suggestions, J. Clean. Prod. 261 (2020) 120813, http://dx.doi.org/10.1016/j.jclepro.2020.120813, URL https://www.sciencedirect.com/science/article/pii/S095965262030860X.

[10] M. Chen, G. Ma, W. Liu, N. Zeng, X. Luo, An overview of data-driven battery health estimation technology for battery management system, Neurocomputing 532 (2023) 152–169, http://dx.doi.org/10.1016/j.neucom.2023.02.031, URL https://www.sciencedirect.com/science/article/pii/S0925231223001686.

[11] S. Pohlmann, A. Mashayekh, F. Stroebl, D. Karnehm, M. Kuder, A. Neve, T. Weyh, State-of-health prediction of lithium-ion batteries based on a low dimensional Gaussian process regression, J. Energy Storage 88 (2024) 111649, http://dx.doi.org/10.1016/j.est.2024.111649, URL https://www.sciencedirect.com/science/article/pii/S2352152X24012349.

[12] H. Nara, T. Yokoshima, T. Osaka, Technology of electrochemical impedance spectroscopy for an energy-sustainable society, Curr. Opin. Electrochem. 20 (2020) 66–77, http://dx.doi.org/10.1016/j.coelec.2020.02.026, URL https://www.sciencedirect.com/science/article/pii/S2451910320300570.

[13] N. Lohmann, P. Weßkamp, P. Haußmann, J. Melbert, T. Musch, Electrochemical impedance spectroscopy for lithium-ion cells: Test equipment and procedures for aging and fast characterization in time and frequency domain, J. Power Sources 273 (2015) 613–623, http://dx.doi.org/10.1016/j.jpowsour.2014.09.132.

[14] L. Xu, Y. Xiao, Y. Yang, S.-J. Yang, X.-R. Chen, R. Xu, Y.-X. Yao, W.-L. Cai, C. Yan, J.-Q. Huang, Q. Zhang, Operando quantified lithium plating determination enabled by dynamic capacitance measurement in working li-ion batteries, Angew. Chem., Int. Ed. Engl. 61 (39) (2022) e202210365, http://dx.doi.org/10.1002/anie.202210365.

[15] N. Meddings, M. Heinrich, F. Overney, J.-S. Lee, V. Ruiz, E. Napolitano, S. Seitz, G. Hinds, R. Raccichini, M. Gaberšček, J. Park, Application of electrochemical impedance spectroscopy to commercial li-ion cells: A review, J. Power Sources 480 (2020) 228742, http://dx.doi.org/10.1016/j.jpowsour.2020.228742, URL https://www.sciencedirect.com/science/article/pii/S0378775320310466.

[16] Y. Li, K. Liu, A.M. Foley, A. Zülke, M. Berecibar, E. Nanini-Maury, J.V. Mierlo, H.E. Hoster, Data-driven health estimation and lifetime prediction of lithium-ion batteries: A review, Renew. Sustain. Energy Rev. 113 (2019) 109254, http://dx.doi.org/10.1016/j.rser.2019.109254, URL https://www.sciencedirect.com/science/article/pii/S136403211930454X.

[17] K.M. Carthy, H. Gullapalli, K.M. Ryan, T. Kennedy, Review—Use of impedance spectroscopy for the estimation of li-ion battery state of charge, state of health and internal temperature, J. Electrochem. Soc. 168 (8) (2021) 080517, http://dx.doi.org/10.1149/1945-7111/ac1a85.

[18] Y. Zhang, Q. Tang, Y. Zhang, J. Wang, U. Stimming, A.A. Lee, Identifying degradation patterns of lithium ion batteries from impedance spectroscopy using machine learning, Nature Commun. 11 (1) (2020) 1706, http://dx.doi.org/10.1038/s41467-020-15235-7.

[19] J. Obregon, Y.-R. Han, C.W. Ho, D. Mouraliraman, C.W. Lee, J.-Y. Jung, Convolutional autoencoder-based SOH estimation of lithium-ion batteries using electrochemical impedance spectroscopy, J. Energy Storage 60 (2023) 106680, http://dx.doi.org/10.1016/j.est.2023.106680, URL https://www.sciencedirect.com/science/article/pii/S2352152X23000774.

[20] B. Jiang, J. Zhu, X. Wang, X. Wei, W. Shang, H. Dai, A comparative study of different features extracted from electrochemical impedance spectroscopy in state of health estimation for lithium-ion batteries, Appl. Energy 322 (2022) 119502, http://dx.doi.org/10.1016/j.apenergy.2022.119502, URL https://www.sciencedirect.com/science/article/pii/S030626192200825X.

[21] H.S. Chan, E.J. Dickinson, T.P. Heins, J. Park, M. Gaberšček, Y.Y. Lee, M. Heinrich, V. Ruiz, E. Napolitano, P. Kauranen, E. Fedorovskaya, J. Moškon, T. Kallio, S. Mousavihashemi, U. Krewer, G. Hinds, S. Seitz, Comparison of methodologies to estimate state-of-health of commercial li-ion cells from electrochemical frequency response data, J. Power Sources 542 (2022) 231814, http://dx.doi.org/10.1016/j.jpowsour.2022.231814, URL https://www.sciencedirect.com/science/article/pii/S0378775322008035.

[22] D. Edelmann, T.F. Móri, G.J. Székely, On relationships between the pearson and the distance correlation coefficients, Statist. Probab. Lett. 169 (2021) 108960, http://dx.doi.org/10.1016/j.spl.2020.108960, URL https://www.sciencedirect.com/science/article/pii/S0167715220302637.

[23] Z. Zhou, Measuring nonlinear dependence in time-series, a distance correlation approach, J. Time Series Anal. 33 (3) (2012) 438–457, http://dx.doi.org/10.1111/j.1467-9892.2011.00780.x.

[24] J. Sun, J. Kainz, State of health estimation for lithium-ion batteries based on current interrupt method and genetic algorithm optimized back propagation neural network, J. Power Sources 591 (2024) 233842, http://dx.doi.org/10.1016/j.jpowsour.2023.233842, URL https://www.sciencedirect.com/science/article/pii/S0378775323012181.

[25] Y. Li, M. Maleki, S. Banitaan, State of health estimation of lithium-ion batteries using EIS measurement and transfer learning, J. Energy Storage 73 (2023) 109185, http://dx.doi.org/10.1016/j.est.2023.109185, URL https://www.sciencedirect.com/science/article/pii/S2352152X23025835.

[26] F. Guo, G. Huang, W. Zhang, G. Liu, T. Li, N. Ouyang, S. Zhu, State of health estimation method for lithium batteries based on electrochemical impedance spectroscopy and pseudo-image feature extraction, Measurement 220 (2023) 113412, http://dx.doi.org/10.1016/j.measurement.2023.113412, URL https://www.sciencedirect.com/science/article/pii/S0263224123009764.

[27] C.M. Bishop, Pattern recognition and machine learning, in: Information Science and Statistics, Springer New York, 2016, URL https://books.google.de/books?id=kOXDtAEACAAJ.

[28] V. Vapnik, The nature of statistical learning theory, in: Information Science and Statistics, Springer New York, 2013, URL https://books.google.de/books?id=EqgACAAAQBAJ.

[29] Q. Li, D. Li, K. Zhao, L. Wang, K. Wang, State of health estimation of lithium-ion battery based on improved ant lion optimization and support vector regression, J. Energy Storage 50 (2022) 104215, http://dx.doi.org/10.1016/j.est.2022.104215, URL https://www.sciencedirect.com/science/article/pii/S2352152X22002468.

[30] X. Tan, D. Zhan, P. Lyu, J. Rao, Y. Fan, Online state-of-health estimation of lithium-ion battery based on dynamic parameter identification at multi timescale and support vector regression, J. Power Sources 484 (2021) 229233, http://dx.doi.org/10.1016/j.jpowsour.2020.229233, URL https://www.sciencedirect.com/science/article/pii/S0378775320315226.

[31] I. Steinwart, A. Christmann, Support vector machines, in: Information Science and Statistics, Springer New York, 2008, URL https://books.google.de/books?id=HUnqnrpYt4IC.

[32] N. Monzen, F. Stroebl, H. Palm, C.M. Hackl, Multiobjective hyperparameter optimization of artificial neural networks for optimal feedforward torque control of synchronous machines, IEEE Open J. Ind. Electron. Soc. 5 (2024) 41–53, http://dx.doi.org/10.1109/OJIES.2024.3356721.

[33] L. Driscoll, S. de la Torre, J.A. Gomez-Ruiz, Feature-based lithium-ion battery state of health estimation with artificial neural networks, J. Energy Storage 50 (2022) 104584, http://dx.doi.org/10.1016/j.est.2022.104584, URL https://www.sciencedirect.com/science/article/pii/S2352152X22006004.

[34] Z. Fan, X. Zi-xuan, W. Ming-hu, State of health estimation for li-ion battery using characteristic voltage intervals and genetic algorithm optimized back propagation neural network, J. Energy Storage 57 (2023) 106277, http://dx.doi.org/10.1016/j.est.2022.106277, URL https://www.sciencedirect.com/science/article/pii/S2352152X22022666.

[35] D.P. Kingma, J. Ba, Adam: A method for stochastic optimization, 2017, arXiv:1412.6980, URL https://arxiv.org/abs/1412.6980.

[36] M.M. Camboim, A.C. Moreira, M. de Fátima N.C. Rosolem, R.F. Beck, V.T. Arioli, C. Omae, H. Ding, State of health estimation of second-life batteries through electrochemical impedance spectroscopy and dimensionality reduction, J. Energy Storage 78 (2024) 110063, http://dx.doi.org/10.1016/j.est.2023.110063, URL https://www.sciencedirect.com/science/article/pii/S2352152X2303462X.

[37] P. Iurilli, C. Brivio, V. Wood, On the use of electrochemical impedance spectroscopy to characterize and model the aging phenomena of lithium-ion batteries: a critical review, J. Power Sources 505 (2021) 229860, http://dx.doi.org/10.1016/j.jpowsour.2021.229860, URL https://www.sciencedirect.com/science/article/pii/S0378775321003992.

[38] Z. Pang, K. Yang, Z. Song, P. Niu, G. Chen, J. Meng, A new method for determining SOH of lithium batteries using the real-part ratio of EIS specific frequency impedance, J. Energy Storage 72 (2023) 108693, http://dx.doi.org/10.1016/j.est.2023.108693, URL https://www.sciencedirect.com/science/article/pii/S2352152X2302090X.

[39] M. Dong, X. Li, Z. Yang, Y. Chang, W. Liu, Y. Luo, W. Lei, M. Ren, C. Zhang, State of health (SOH) assessment for LIBs based on characteristic electrochemical impedance, J. Power Sources 603 (2024) 234386, http://dx.doi.org/10.1016/j.jpowsour.2024.234386, URL https://www.sciencedirect.com/science/article/pii/S0378775324003379.